

Supporting information for:

Hybrid Plasmonic Bullseye Antennas for Efficient Photon Collection

Sebastian K. H. Andersen,^{*,†} Simeon Bogdanov,[‡] Oksana Makarova,[‡] Yi Xuan,[‡] Mikhail Y. Shalaginov,[‡] Alexandra Boltasseva,[‡] Sergey I. Bozhevolnyi,[†] and Vladimir M. Shalaev[‡]

[†]*Center for Nano Optics, University of Southern Denmark, DK-5230 Odense M, Denmark*

[‡]*School of Electrical and Computer Engineering, Purdue Quantum Center, Purdue University, West Lafayette, Indiana 47907, USA*

E-mail: sekh@mci.sdu.dk

Sample Preparation

The bullseye antenna was fabricated by successive electron-beam evaporation of 10 nm Ti, 3 nm Ge, 200 nm Ag topped by 15 nm SiO₂ on a Si wafer, at a deposition rate of \sim 1 Å/s and 10⁻⁶ mbar chamber pressure, without breaking the vacuum. The Ge layer act as a wetting layer, reducing roughness of the consecutively deposited Ag film.^{S1} PMMA 4A was subsequently spincoated at 4000 rpm on the sample, and prebaked at 180 C° for 3 min before patterning by a 100kV electron beam lithography system (Leica VB6). After development (1:3 MIBK-to-IPA for 1 min followed by 1 min rinse in IPA), a 100 nm TiO₂ layer was deposited by electron-beam evaporation at \sim 1 Å/s and 10⁻⁶ mbar pressure. Lift-off in acetone at 60 C° for 5 h was partially successful, as subsequently 5 min of sonication in acetone was

required to remove PMMA between the TiO_2 ridges to reveal the bullseye. In preparation of ND placement, 100 nm ND's containing ~ 400 NV-centers (Adamas technology) was spin-coated on a coverslip, previously cleaned in piraniha etch (Nanostrip x2 - KMG electronic chemicals). To ease the transfer, the bullseye sample was coated with a ~ 2 nm thick layer of positively charged poly-allylamine hydrochloride (PAH) layer. ND pick-up was performed by a force curve sequence, with the AFM cantilever situated above the ND. Successful pick-up was confirmed by a subsequent non-contact scan. Exchanging samples, a force curve was performed in the center of the bullseye, followed by an AFM scan to confirm the placement of the ND.

Numerical Modelling

Numerical modelling was performed in the commercially available Comsol Multiphysics 5.1. The full 3-D field of the axial symmetric system is numerically modelled by solving a 2-D slice, on the assumption of a constant azimuthal phase. The limited computational requirements of 2-D modelling, allowed us to model the full bullseye antenna, in a domain of radius $22\mu\text{m}$, bounded from the top by a perfectly matched layer and below by the silver film. Material parameters for silver were obtained for tabulated data,^{S2} while TiO_2 data was measured by ellipsometry (see figure S4) and a refractive index of 1.45 was set for SiO_2 . The emission field was generated by an electric dipole source positioned on the symmetry axis, 15 nm above the SiO_2 film. The decay rate enhancement was obtained as the total power dissipated by the dipole in the bullseye environment, relative to that of free space. Collection efficiency was obtained as the power integrated over a 0.9 NA collection surface, relative to the total power dissipated by the dipole. The radiation pattern was obtained by plotting the normal component of the Poynting vector over a circular arc in the 2-D plane, centered on the dipole. A large arc radius of $20\mu\text{m}$ was necessary in order to reach a convergent solution of the emission pattern. Knowing the radius of the circular path and the arc length with respect to zero degree out of plane, the angle of emission for a particular point could easily

be calculated.

Experiment

The ND was excited with a 532 nm continuous wave laser, focused onto the sample by a 0.9 NA $\times 100$ objective which was mounted on a piezo-stage for fine positioning of laserspot. Fluorescence collected by the same objective was filtered by a 550 nm dichroic mirror (DMLP550L-Thorlabs) and 550 nm long pass filter (FEL0550- Thorlabs), before being directed to a spectrometer (QE65000 - Ocean Optics) or avalanche photodiode (SPCM-AQRH - Excelitas) in a confocal detection configuration using a $50 \mu m$ pinhole. Alternatively fluorescence was detected by a charge coupled camera (414Ex - Atik Cameras) imaging sample plane (using a 20 mm tube lens) or back-focal plane (600 mm bertrand- and 75 mm tube lens) onto the camera. off- or on-resonance emission was selected by filters of respectively 560-610 nm and 650-740 nm transmission bands, while an analyzer (LPVISC050-MP2 - Thorlabs) was introduced to probe polarization. Back-focal plane images from bullseye antenna, was background corrected for a corresponding image from an empty antenna. Saturation curve measurement was performed with a ND2 filter positioned in front of the avalanche photodiode, the presented count rate was corrected for transmission of ND2 filter and the pinhole. The experimental setup is given in figure S1.

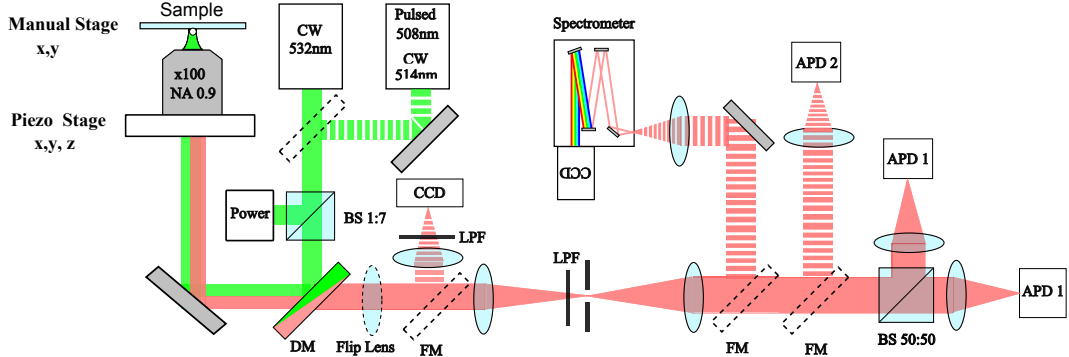


Figure S1: Schematic of experimental setup applied for characterization of emission properties of ND in bullseye antenna. DM: Dichroic mirror, FM: Flip mirror, APD: avalanche photodiode, CCD: charge coupled device, BS: Beamsplitter. The 532 nm CW pump laser was used for excitation of NV-centers, through the NA 0.9 x100 Objective. Fluorescence collected by the same objective, was imaged onto the CCD camera, spectrally resolved on the spectrometer or detected by APD2 for saturation curve measurement. For back-focal plane imaging, a flip lens was introduced before the CCD.

Dipole above plane silver film

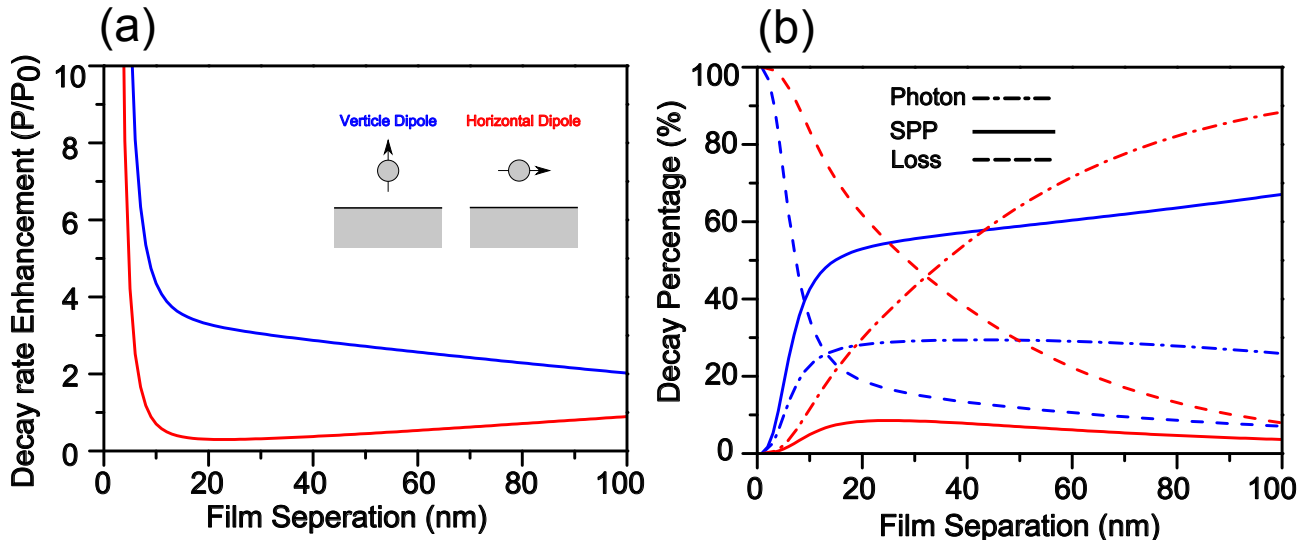


Figure S2: Analytical model for dipole emission above an infinite silver film, emitting at a wavelength of 670 nm. For dipole oriented verticle (blue) or horizontal (red). (a) Power dissipated by dipole relative to vaccum. The emission is suppressed for a horizontal dipole in close proximity (~ 30 nm) to the silver film (b) Relative decay rates into photons (dash-dot), SPP (solid) and quenching (dashed). The verticle dipole couples efficiently to SPP. Modelling is reproduced based on the analytical model developed in reference.^{S3}

Ellipsometry Measurement of TiO₂ film

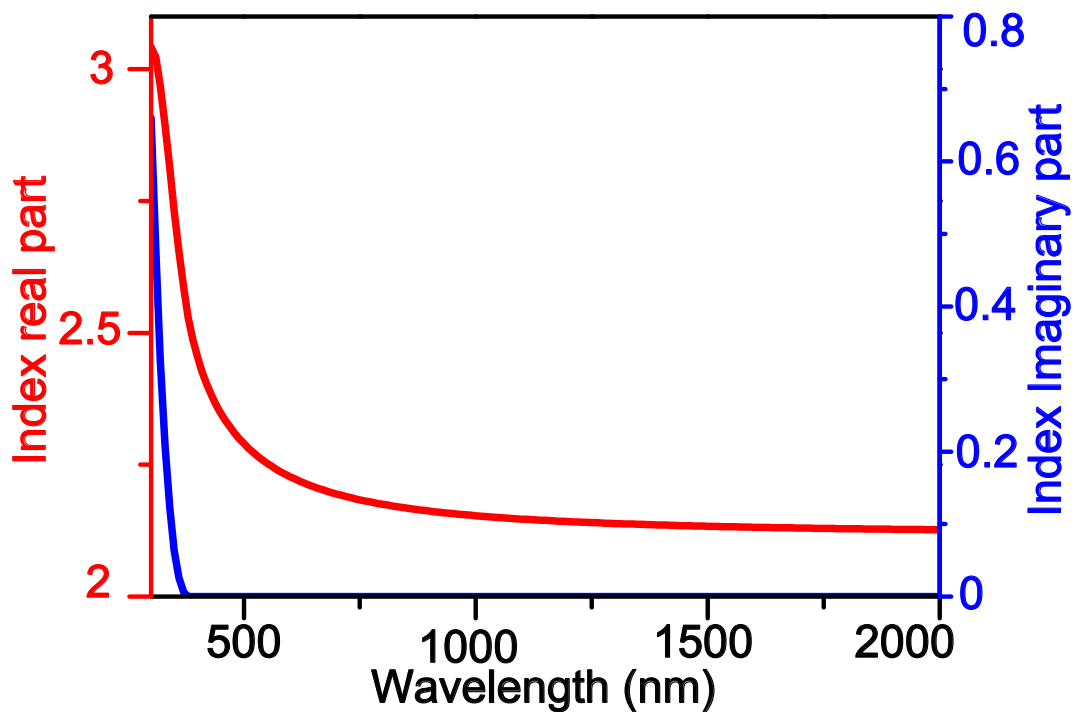


Figure S3: Ellipsometry measurement of 100 nm TiO₂ film deposited by e-beam evaporation on Si substrate. The measurement is applied for numerical modelling of TiO₂ film.

Numerical Optimization Procedure

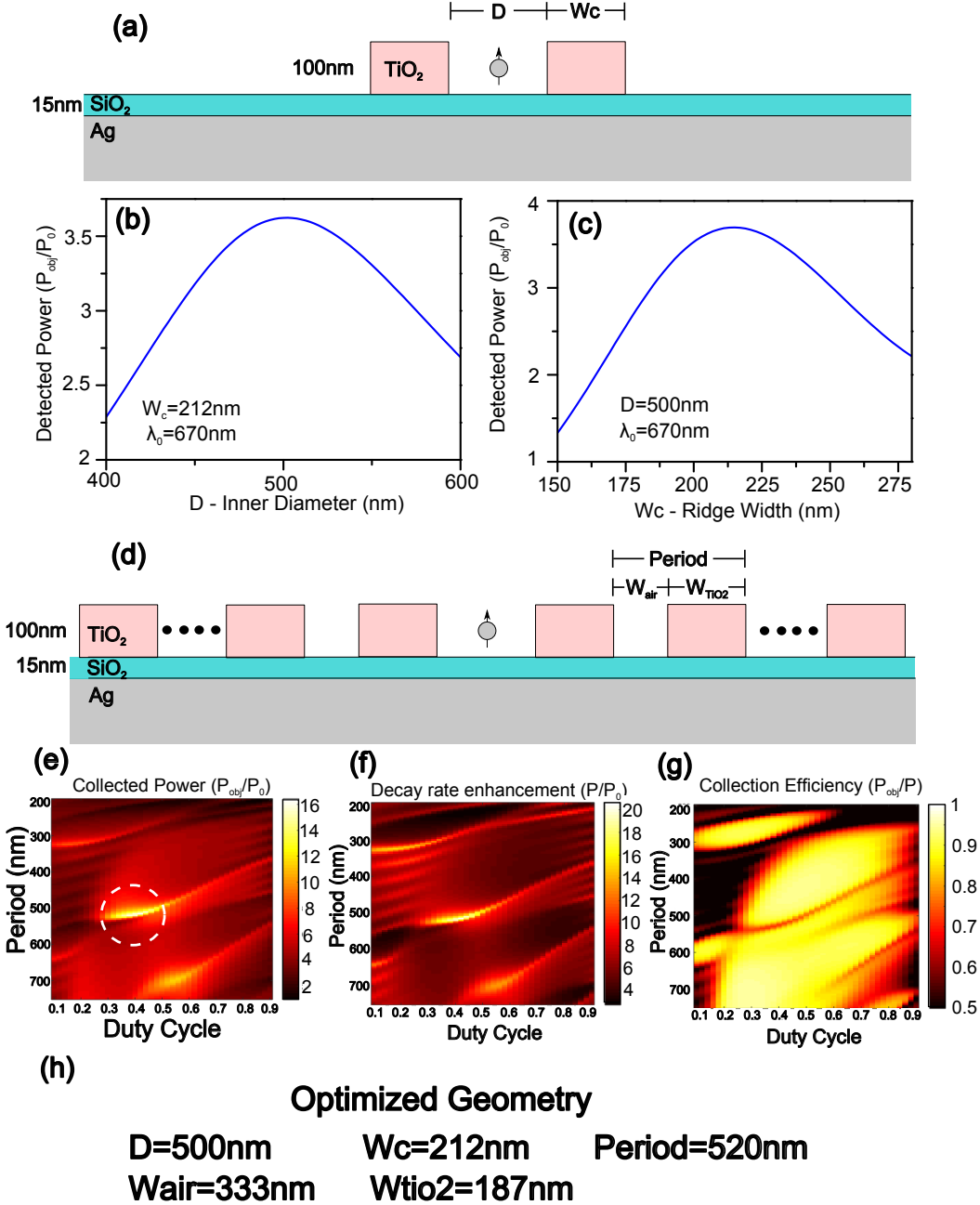


Figure S4: Numerical optimization procedure for bullseye antenna targeted for emission wavelength 670 nm (a) A single TiO_2 ridge is initially optimized for maximum dipole power radiated to the objective. (b,c) The parameters of inner diameter (D) and TiO_2 ridge width (W_c) is interatively optimized until a self-consistent maxima is reached. (d) The 7 ridge grating, geometrically described by period and duty cycle, is then added. (e) Mapping the dipole power collected by the objective as a function of period and duty cycle the optimal grating configuration is determined. (f,g) The corresponding maps of decay rate enhancement and collection efficiency is included to illustrate their invers relationship. (h) List of optimized parameters.

Antenna performance vs dipole height

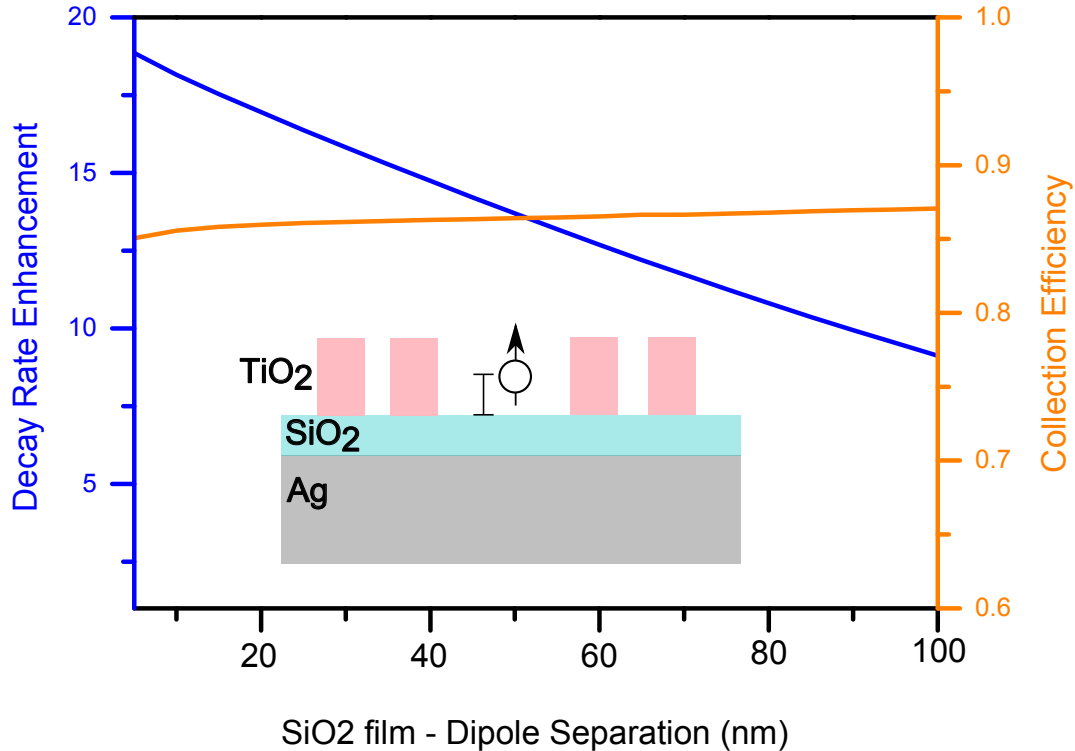


Figure S5: Decay rate enhancement (blue) and collection efficiency (orange) as function of dipole height, above the SiO₂ film. The dipole response is modelled for a verticle dipole, emitted at a wavelength of 670 nm positioned on the symmetry axis of the bullseye antenna optimized in figure S4.

Comparision of emission pattern with grating equation

In the following, the numerically modelled emission pattern is compared with the grating equation (eq 1), describing the condition for coupling propagating surface plasmon polaritons to free space radiation.

$$k_{spp} = k_\sigma \pm nG \quad n = \pm 1, 2, 3, 4\dots \quad (1)$$

$G = \frac{2\pi}{\Lambda}$ being the grating vector with period Λ , $k_\sigma = k_0 \sin(\theta)$ being the in-plane wavevector of free radiation propagating along emission angle θ and $k_{spp} = k_0 N_{eff}^G$ SPP wavevector.

For the dielectric grating we describe N_{eff}^G , weighted by grating fill factor.

$$N_{eff}^G = \chi N_{eff}^{TiO_2} + (1 - \chi) N_{eff}^{Air} \quad (2)$$

$N_{eff}^{TiO_2} = 2.25$ being the SPP effective index for the TiO_2 - SiO_2 -Ag layer structure and $N_{eff}^{Air} = 1.05$ for the Air₂- SiO_2 -Ag profile, modelled by the 3-layer dispersion relation for the design wavelength of 670 nm and $\chi = 0.36$ the grating duty cycle for the optimized bullseye design. The numerically modelled bullseye emission generally follow the trends of the grating equation (Figure S4).

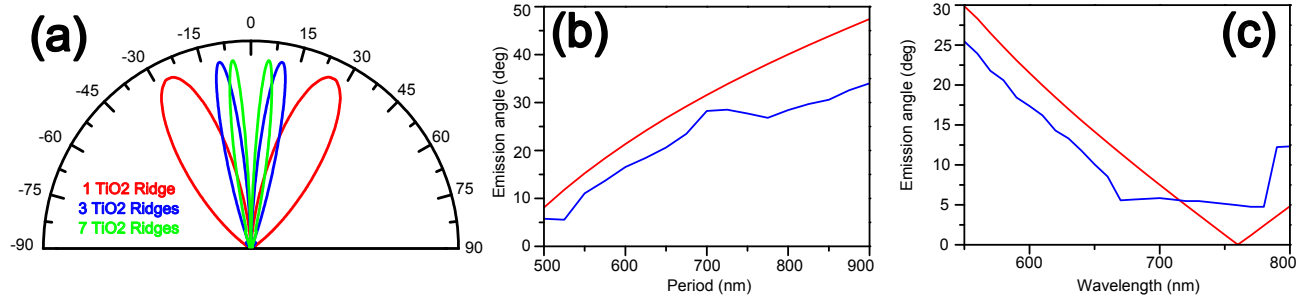


Figure S6: Emission pattern modelled for the optimized bullseye design at the target wavelength $\lambda_0 = 670$ nm. (a) Emission pattern as function of number of TiO_2 ridges, the emission pattern becomes increasingly directional with increasing number of ridges. Numerically modelled angle of maximum emitted power for optimized bullseye design (blue) and comparison with emission angle calculated with grating equation (red).(b) as a function of grating period or (c) vacuum wavelength.

Optimization for different TiO₂ heights

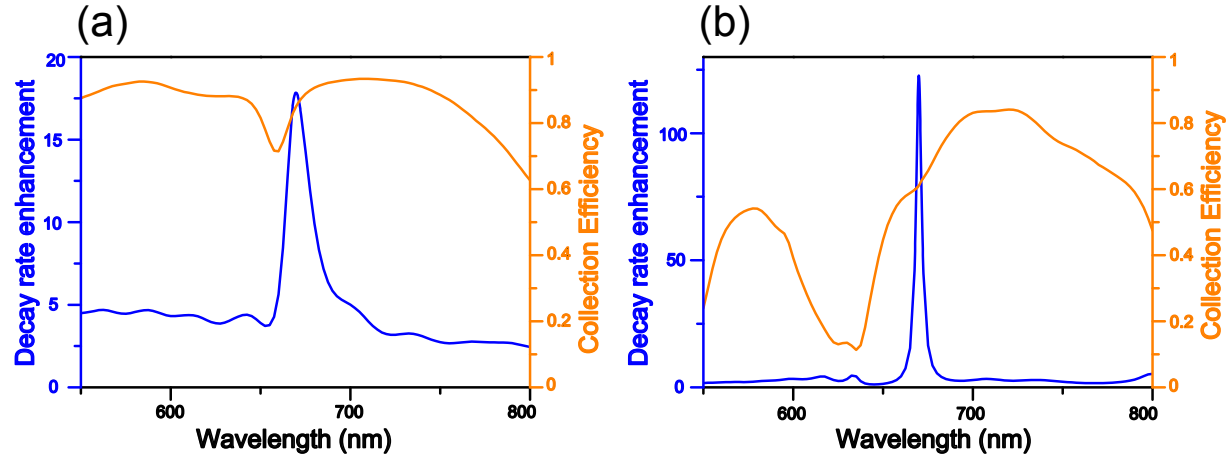


Figure S7: Modelled decay rate enhancement (blue) and collection efficiency (Orange) for (a) design optimized in figure S4 at a TiO₂ height of 100 nm and SiO₂ thickness of 15 nm. (b) Alternative design optimized for TiO₂ height of 260 nm and 15 nm SiO₂ thickness. Increasing TiO₂ height increase SPP reflectivity of the TiO₂ ridges, leading to a larger cavity Q-factor and increased decay rate enhancement, at the cost of collection efficiency as the SPP perform an increasing number of lossy, standing wave, round trips before scattering to free space.

Fluorescence image of bullseye antenna in log scale

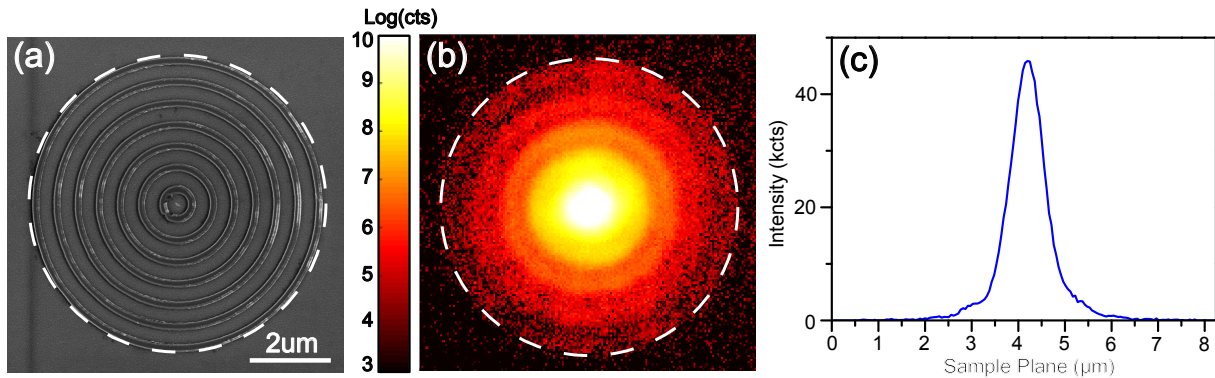


Figure S8: (a) Scanning electron micrograph of bullseye antenna containing single nanodiamond. (b) Corresponding fluorescence image in log scale, dashed line indicate boundary of bullseye antenna, measured with 550 nm long pass filter. The linear scale version of the image appearing in the article figure 2d. (c) Intensity profile through center of image in b.

Confocal scans of bullseye antennas

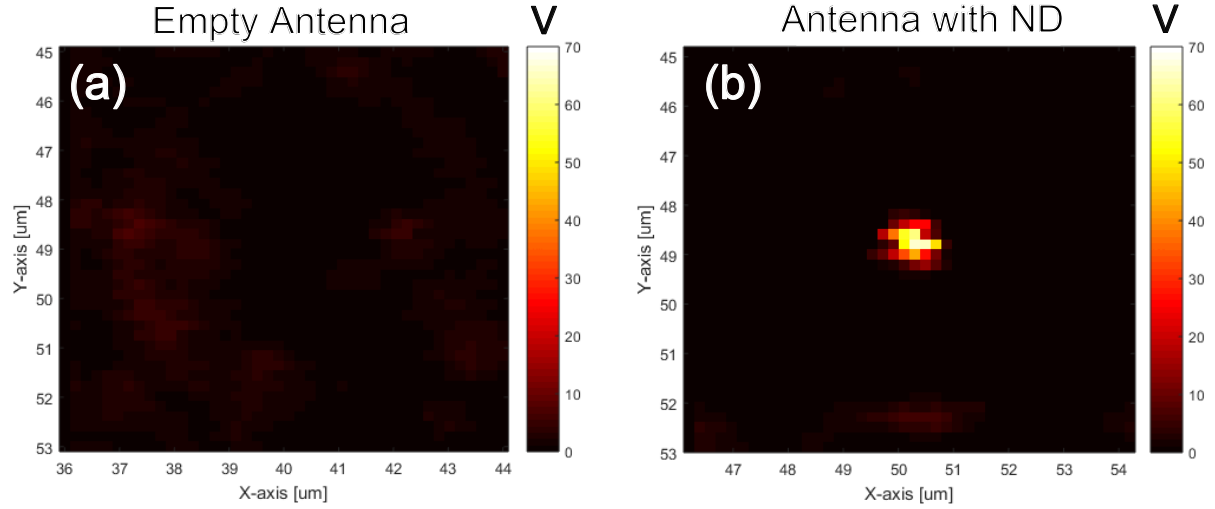


Figure S9: Confocal scan of (a) empty bullseye antenna and (b) bullseye antenna containing a fluorescent ND. Scanned with 532 nm pump laser at $100\mu W$. Scale bar is identical for both images.

Lifetime distribution of NV-centers in nano diamonds

Lifetime decay curves ($I(t)$) are measured by a 1MHz pulsed excitation at a wavelength of 508 nm. For the nano diamond in the bullseye antenna or same type of nano diamond on a glass coverslip. As the nano diamonds contain on average 400 NV-centers, the lifetime decay curve consist of distribution of single exponential decays for the individual NV-centers. The lifetime distribution is extracted by fitting a stretched exponential to the decay curve (figure S10a).

$$I(t) = e^{(t/\tau_0)^\beta} = \int_0^\infty P(s, \beta) e^{-st/\tau_0} ds \quad ; \quad s = \tau_0/\tau \quad (3)$$

β and τ_0 being the fitting parameters and P being the probability of finding an NV-center with a lifetime τ . Following the work of Johnton,^{S4} P is given by.

$$P(s, \beta) = \int_0^{\infty} e^{-u^{\beta} \cos(\pi\beta/2)} \cos(su - u^{\beta} \sin(\pi\beta/2)) du \quad (4)$$

Figure S10b, give the lifetime probability distribution for the nanodiamond in the antenna and distributions from nanodiamonds on glass. While significant variations in lifetime distributions is observed between individual nano diamonds on glass, the broadest lifetime distribution is observed for nano diamond in the antenna.

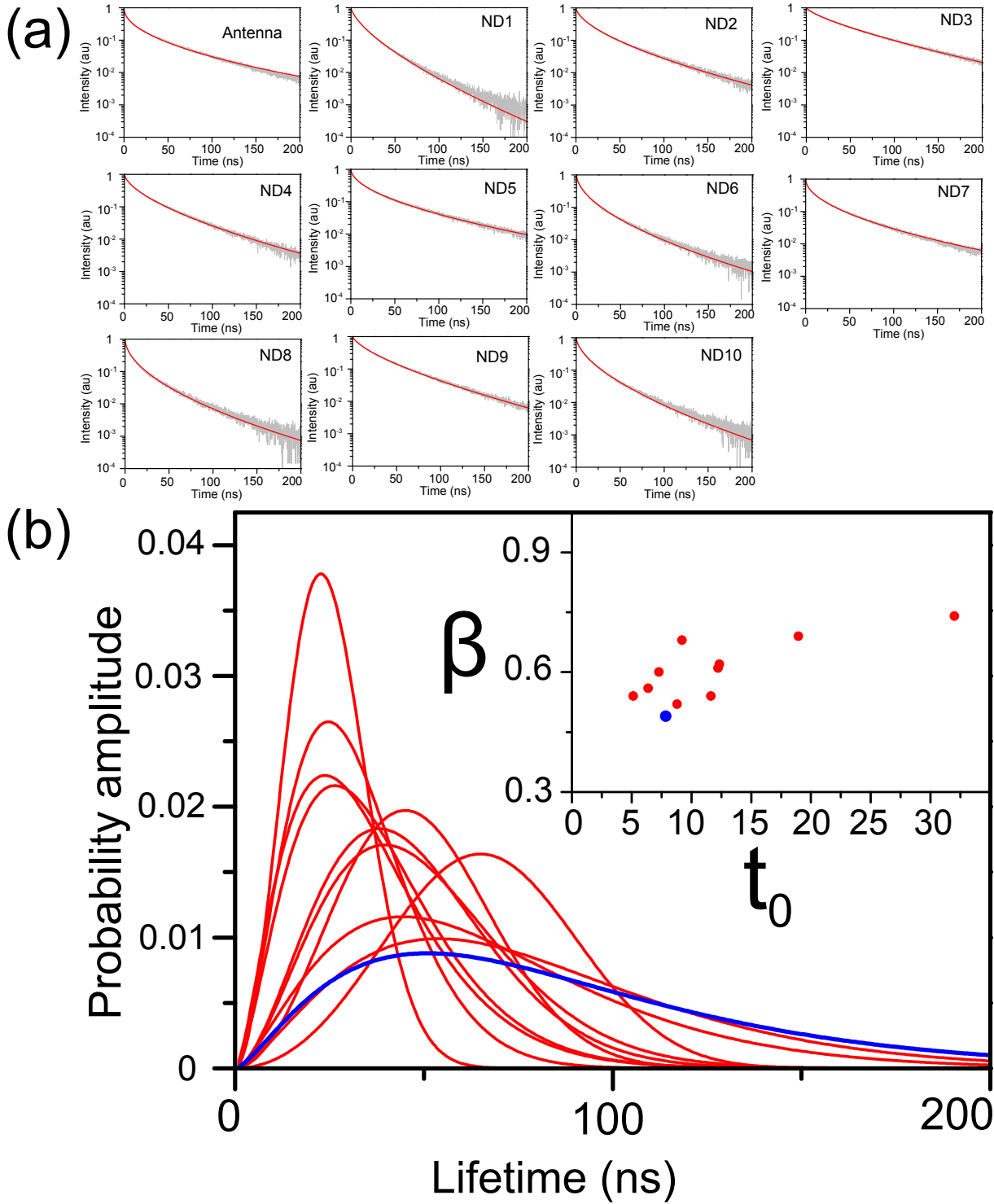


Figure S10: (a) Lifetime measurements of ND in antenna, and 10 nanodiamonds of the same type spincoated on a glass coverslip, ND1 to ND10. Experimental data(grey) and stretched exponential fit (red). (b) Lifetime distributions extracted from stretched exponential fits, for nanodiamond in antenna(blue) and nanodiamonds on glass. Inset give corresponding β - and t_0 -value of stretched exponential fits.

References

- (S1) Chen, W.; Thoreson, M. D.; Ishii, S.; Kildishev, A. V.; Shalaev, V. M. *Opt. Express* **2010**, *18*, 5124–5134.
- (S2) Johnson, P. B.; Christy, R. W. *Phys. Rev. B* **1972**, *6*, 4370–4379.
- (S3) Ford, G.; Weber, W. *Physics Reports* **1984**, *113*, 195 – 287.
- (S4) Johnston, D. C. *Phys. Rev. B* **2006**, *74*, 184430.